NANO LETTERS

Letter

pubs.acs.org/NanoLett

Ultralow Thermal Conductivity of Multilayers with Highly Dissimilar Debye Temperatures

Edward Dechaumphai,[†] Dylan Lu,[‡] Jimmy J. Kan,[§] Jaeyun Moon,[∥] Eric E. Fullerton,*[,‡,§] Zhaowei Liu,*[,‡,§,∥] and Renkun Chen*[,†,∥]

[†]Department of Mechanical and Aerospace Engineering, University of California at San Diego, La Jolla, California 92093, United States

[‡]Department of Electrical and Computer Engineering, University of California at San Diego, La Jolla, California 92093, United States

[§]Center for Magnetic Recording Research, University of California at San Diego, La Jolla, California 92093, United States

[∥]Materials Science and Engineering Program, University of California at San Diego, La Jolla, California 92093, United States

Supporting Information

ABSTRACT: Thermal transport in multilayers (MLs) has attracted significant interest and shows promising applications. Unlike their single-component counterparts, MLs exhibit a thermal conductivity that can be effectively engineered by both the number density of the layers and the interfacial thermal resistance between layers, with the latter being highly tunable via the contrast of acoustic properties of each layer. In this work, we experimentally demonstrated an ultralow thermal conductivity of 0.33 ± 0.04 W m^{-1} K^{-1} at room temperature in MLs made of Au and Si with a high interfacial density of ∼0.2 interface nm^{-1}. The measured thermal conductivity is significantly lower than the amorphous limit of either Si or Au and is also much lower than previously measured MLs with a similar interfacial density. With a Debye temperature ratio of ∼3.9 for Au and Si, the Au/Si MLs represent the highest mismatched system in inorganic MLs measured to date. In addition, we explore the prior theoretical prediction that full phonon dispersion could better model the interfacial thermal resistance involving materials with low Debye temperatures. Our results demonstrate that MLs with highly dissimilar Debye temperatures represent a rational approach to achieve ultralow thermal conductivity in inorganic materials and can also serve as a platform for investigating interfacial thermal transport.

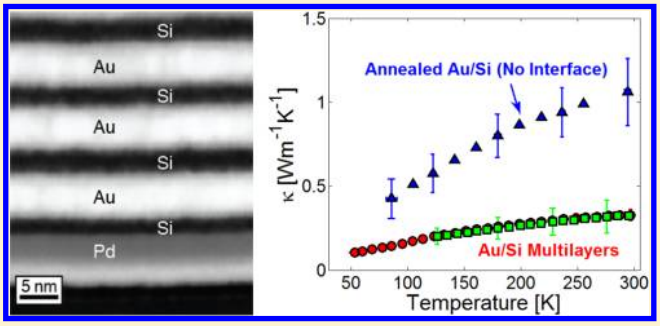

KEYWORDS: *Phonon transport, amorphous limit, diffusive mismatch model, Debye temperature, superlattice*

Thermal transport phenomena in multilayers (MLs) have attracted recent interest due to the pronounced effects of interfacial thermal resistance (ITR) on the overall device performance. For instance, the low thermal conductivity (κ) in MLs caused by ITR could be undesirable in tunnel junctions since inefficient heat dissipation across the junction can cause the degradation of the thin barrier coating and adversely affect device performance.[1] Heat dissipation in MLs used in extreme ultraviolet (EUV) and soft X-ray mirrors can also be a concern.[2,3] On the other hand, a low κ is preferred for applications such as thermal insulation[4] and thermoelectrics.[5−7] Driven by these important implications, several ML systems with a high interfacial density have been measured and show low thermal conductivity values. Examples include $Ge_2Sb_2Te_5$/ZnS:SiO_2 MLs,[8] W/Al_2O_3 nanolaminates,[4] Ta/TaO_x tunnel junctions,[1] CuPC/Ag MLs,[9] Mo/Si MLs,[2,3] and very recently, hybrid organic−inorganic zincone thin films.[10] Nanocrystal arrays (NCAs)[11] and organoclay nanolaminates[12] are also other recently researched materials, which exploit high ITR to produce low κ values of 0.1−0.3 W m^{-1} K^{-1} and 0.06−0.1 W m^{-1} K^{-1} respectively.

MLs also serve as a unique model system for investigating thermal transport across solid−solid interfaces, as thermal properties of MLs can be engineered by selecting an appropriate pair of material systems. Several reports on low thermal conductivity ML systems have shown that ITR dominates the overall behavior of cross-plane thermal transport.[1,2,4,8−10] Costescu et al. reported an ultralow κ of ∼0.6 W m^{-1} K^{-1} at room temperature in W/Al_2O_3 nanolaminates with interfacial density of 0.345 nm^{-1} (ref 4). They also showed that κ of nanolaminates decreases with increasing interfacial density. Here, following Cahill and co-workers,[13] we use "ultralow" to describe a κ value lower than what is predicted by the minimum κ model developed by Cahill et al.[14] Recently, Li et al.[2] reported that the phonon is the dominant heat carrier in Mo/Si MLs,

Received: January 11, 2014
Revised: April 7, 2014
Published: April 14, 2014

   dx.doi.org/10.1021/nl500127c | *Nano Lett.* 2014, 14, 2448−2455

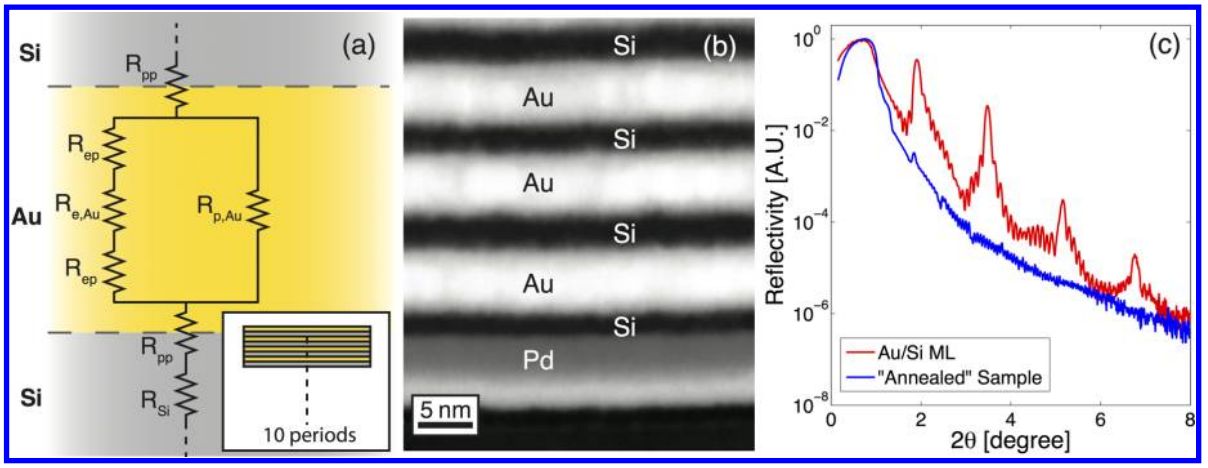

Figure 1. (a) A schematic of the thermal resistive network of the Au/Si ML system. Inset: basic schematic of Au/Si MLs. The thermal resistive network composes of thermal resistances of the Si layer (R_{Si}), Au layer, and interfaces (R_{pp}) connected in series. The Au layer has two thermal pathways in parallel: electron and phonon pathways. The electron pathway includes electron−phonon coupling (R_{ep}) and electron-contributed ($R_{e,Au}$) thermal resistances of Au in series, while the phonon pathway only has a phonon-contributed thermal resistance of Au ($R_{p,Au}$). (b) Dark-field scanning transmission electron microscope (STEM) images of Au/Si MLs. Each Au and Si layers are 5.7 and 3.0 nm, respectively. (c) X-ray reflectivity (XRR) data of Au/Si ML and the "annealed" sample. Peaks in the XRR plot (c) are an indication of the periodicity in Au/Si ML sample. In the annealed sample, no peaks are shown, which is evidence of degradation of Au−Si interfaces after annealing at 550 K for 24 h.

while electron−phonon coupling provides additional thermal resistance in the electron thermal pathway in a thin metal layer.

In addition to MLs, several experiments on the ITR of individual interfaces between two dissimilar materials have shown high ITR in highly mismatched materials.[15−20] Specifically, when the phonon is the dominant heat carrier, the ITR is dictated by the contrast in acoustic properties of the pair materials, which can be characterized by the "Debye temperature ratio" (DTR), or the ratio between the high and low Debye temperatures (θ_D) of the corresponding materials. For instance, Lyeo and Cahill[15] showed that interfaces between materials with high DTRs have high ITRs such as Pb/Si, Bi/Si, Pb/diamond, and Bi/diamond. The thermal conductance of the Bi/hydrogen-terminated diamond, with a DTR of ∼18.7, was measured to be as low as 8.5 MW m^{-2} K^{-1} at room temperature,[15] where the interface between TiN/MgO, both with a similar θ_D, was measured to be 2 orders of magnitude higher, ∼700 MW m^{-2} K^{-1} (ref 16). This suggests that ITR is highly dependent on the DTR. Also, they showed that Bi (semimetal) and Pb (metal), both "soft" materials, yield a similar thermal conductance when paired with the identical "hard" material such as diamond, which suggests that electrons do not play a significant role in interfacial heat transport in those interfaces.[15]

Previous literature discussed above suggests that interfaces between materials with a high DTR would possess a high ITR, and if combined with a high interfacial density in MLs, one would expect a low κ. However, the largest DTR in inorganic ML systems measured to date is about 2.1 for W/Al_2O_3 with the lowest κ of 0.53 W m^{-1} K^{-1} (ref 4). Kim et al. observed a lower κ in GeSbTe based MLs,[8] but the low κ is predominately originated from the GeSbTe and ZnS:SiO_2 layers rather than the interfaces (i.e., the observed κ is still higher than the amorphous limit, or not "ultralow"). A very recent study by Yang and co-workers showed an ultralow κ of 0.13 W m^{-1} K^{-1} in organic/inorganic hybrid MLs,[10] presumably also caused by the low Debye temperature in the organic component. Therefore, one could potentially further reduce κ in inorganic MLs with one of the layers made of a low-θ_D material.

To see the effect of large ITR on the thermal conductivity of a multilayer system, the interfacial density must be sufficiently high. One of the main challenges in the past in realizing inorganic MLs with high DTRs lies in the difficulty of making ML films with distinct sub-10 nm periodic thickness, especially for soft materials. In this work, we achieved MLs with a high interfacial density and a high DTR in Au/Si MLs with sub-10 nm periodic thickness. With a DTR of ∼3.9 (θ_{Au} = 165 K, θ_{Si} = 640 K),[21] the thermal conductivity of the Au/Si MLs was found to be as low as 0.33 ± 0.04 W m^{-1} K^{-1} at room temperature, significantly lower than the amorphous limit of either Si or Au. These results are much lower than previously measured MLs with a similar interfacial density but lower DTRs, demonstrating that one can achieve ultralow thermal conductivity in inorganic MLs with a high DTR. In addition, in accordance with a prior theoretical prediction by Reddy et al.,[22] our experimental data and analysis show that the Debye approximation, which has been commonly used to estimate the ITR, is not valid for materials with a low θ_D, such as Au. Moreover, because both Au and Si are well-studied materials especially with regards to phonon transport, in comparison to a more complex organic/inorganic ML, the Au/Si ML is a simple system (yet challenging to fabricate) with highly mismatched materials for understanding interfacial thermal transport and achieving ultralow thermal conductivity.

Experimental Section. The Au/Si MLs were grown at room temperature under high vacuum by DC magnetron sputtering onto Si substrates. The base pressure of the chamber was 5 × 10^{-8} Torr, and the Ar sputtering gas pressure was fixed at 2.5 mTorr. Sputtering rates for Au at 50 W (∼2.5 W cm^{-2}) and Si at 100 W (∼5 W cm^{-2}) were 1.1 Å s^{-1} and 0.19 Å s^{-1}, determined by X-ray reflectivity measurements of calibration film sample thicknesses. Portions of 2 nm of Ta and 3 nm of Pd were deposited prior to Au and Si to promote adhesion of the multilayer structure to the Si substrate. Au/Si MLs are composed of 10 periods with a total thickness of 87 nm, where the layer thicknesses of the Au and Si layers are 5.7 and 3.0 nm, respectively. The layer thickness was determined by the dark-field scanning transmission electron microscope (STEM)

dx.doi.org/10.1021/nl500127c | Nano Lett. 2014, 14, 2448−2455

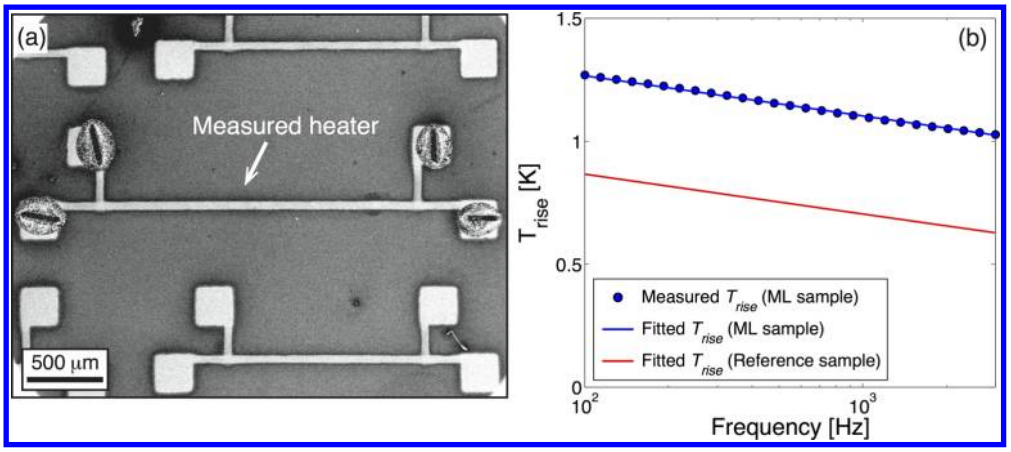

Figure 2. (a) A scanning electron microscopic (SEM) image of 3ω heater for κ measurement. (b) Plot of temperature rise (T_{rise}) as a function of frequency obtained from 3ω measurement. From the measured T_{rise} of reference sample (substrate + insulation layer) and ML sample (substrate + insulation layer + ML film), the 2D heat conduction model is employed to determine κ of the ML film by fitting the calculated T_{rise} with the measured values. Blue dots are an example of measured T_{rise} data of the ML sample, while the blue and red lines are the fitted T_{rise} from the 2D heat conduction model of the reference and ML samples, respectively. The difference between the blue and red lines represents the T_{rise} contributed by the ML film only. Fitting for reference sample is shown in the Supporting Information S1.

imaging of the multilayer cross section (Figure 1b). The well-formed periodic structure with a highly conformal coating across the substrate is evident from both the STEM images and the X-ray reflectometry (XRR) data shown in Figure 1c. Satellite peaks resulting from finite-size effects appear next to the Bragg-like superlattice peaks. This is an indication that the Au−Si interfaces are very smooth and crystalline coherence is maintained through the structure.

A frequency domain differential 3ω method was employed[23,24] to measure the cross-plane κ of the MLs. In a typical 3ω experiment, a thermal wave from Joule heating penetrates into the material, where its penetration depth depends on the thermal diffusivity of the material. Our 3ω heaters were fabricated by the sputtering of Ti (as an adhesion layer) and Au using a stainless steel shadow mask, as shown in Figure 2a. To ensure that no electrical current leaks through the measured film, Al_2O_3 thin film (~235 nm) was deposited as an electrical insulation layer between the heater and the MLs using atomic layer deposition (ALD) at 100 °C. A high-temperature process was avoided because it would anneal the ML samples and cause interdiffusion between layers. In this experiment, we used a current source (Keithley 6221) modulated at 1ω to generate Joule heating on a 3ω metal strip of 2.3 mm long and ~50 μm wide.

The temperature rise across the ML film is isolated from the substrate and insulation layer via a differential method, where the difference in temperature rises between the reference sample (substrate + insulation layer) and the ML sample (substrate + insulation layer + ML film) is taken over a frequency range resulting in a temperature rise contributed by the film. Because the heater width (~50 μm) is much larger than the thickness of the MLs (87 nm), lateral heat spreading is minimal, and the cross-plane measurement is not affected by the anisotropic property of Au/Si ML, as confirmed by our numeric simulation of the heat transfer process. In our experiments, the heater width can vary from sample to sample, leading to slightly different heat fluxes. To accurately determine the temperature rise contributed by the ML film only, a generalized 2D heat conduction model was employed.[25,26] Note that simply normalizing the temperature rise to account for heater width variation is not strictly accurate since heater width b is within the integral part of the frequency domain 2D heat conduction equation.[25] In this 3ω scheme using 2D heat conduction analysis, the reference sample is measured to obtain the temperature rise as a function of frequency. The heat conduction model is then applied to find κ of both substrate and insulation layers by fitting the model with the measured temperature rise of reference sample. These fitted parameters are then applied to the ML samples, leaving only one fitting parameter, κ_{ML}, as shown in Figure 2b. This procedure assumes that the thicknesses and thermal conductivities of substrate and insulation layers in both the reference and the ML samples are identical. Therefore, to minimize variations of these parameters between reference and ML samples, all sample preparations and fabrication processes underwent the same conditions at the same time. The additional interfacial thermal resistances between the insulation layer and the ML film as well as between the ML film and its wetting layer are omitted in the experimental data analysis for simplicity since these resistances are much smaller than the total thermal resistance of the ML film (see the Supporting Information S2). If these additional thermal resistances were included, the measured κ would be at most 5.1% higher, which is within the uncertainty of the 3ω measurements. Also, κ measurements were prepared and performed right after MLs fabrication since Au/Si interfaces can deteriorate over time[27,28] (see the Supporting Information S3).

Results and Discussion. The measured temperature dependent cross-plane thermal conductivity data on Au/Si MLs are summarized in Figure 3. ML samples #1 and #2 are from different locations of the same wafer; the measured κ between these two samples are similar, thereby verifying that the Au/Si MLs are homogeneous across the wafer. At room temperature, the κ of the Au/Si MLs is 0.33 ± 0.04 W m^{-1} K^{-1}, which is even lower than their amorphous thin film counterparts (amorphous lattice thermal conductivity κ_L for Si and Au are 1.05−1.6 and 0.49 W m^{-1} K^{-1}, respectively[5,14,29−31]). The κ of Au/Si MLs retains an increasing temperature tendency from 50 to 300 K, similar to previously observed measurements on interfacial thermal conductance.[15,16]

dx.doi.org/10.1021/nl500127c | Nano Lett. 2014, 14, 2448−2455

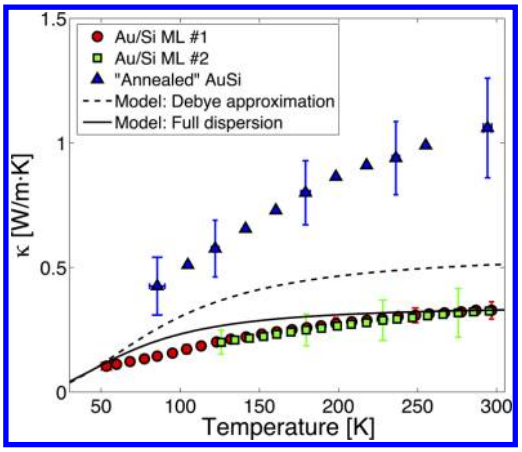

Figure 3. Thermal conductivity of Au/Si ML (red circles and green squares) and the "annealed" Au−Si (blue triangles) samples as a function of temperature. A much higher thermal conductivity in the annealed sample, in which the interfaces were absent, demonstrates the importance of thermal boundary resistance to the thermal transport in MLs. The modeling result based on the full phonon dispersion (solid line) agrees with the experimental data much better than that based on the Debye approximation (dash line), suggesting the advantage of using full dispersion for low Debye temperature materials such as Au.

The observed low κ in the MLs can be associated with the high ITR between the Au and Si interfaces. To elucidate this premise, another 3ω measurement was performed on a sample of an identical Au/Si ML that has been annealed at high temperature. The annealing process was performed in the Ar environment at 550 K for 24 h, which is sufficient to result in interdiffusion between layers or alloy formation at the interface.[22,23] As a result, the distinct interfaces between Au and Si in the "annealed" sample are eliminated, as confirmed by the XRR data, where the immense dampening of the Bragg-like peaks exhibits the degradation of the ML (Figure 1c). At room temperature, κ of the annealed sample is 1.06 ± 0.20 W m^{-1} K^{-1}, which is more than three times larger than the MLs. An increase in κ after annealing indicates that high thermal boundary resistance in the original MLs is prompted by the distinct interfaces between Au and Si.

To understand the thermal data of the MLs, a basic thermal network model is implemented to elucidate thermal transport mechanism in the ML structure as shown in Figure 1a. The model is simplified by neglecting the Au/Si interdiffusive layer. The effective thermal conductivity of the film then can be described as

$$\kappa = \frac{d_{Au} + d_{Si}}{R_{unit}} \tag{1}$$

in which

$$R_{unit} = R_{Si} + \left(\frac{1}{2R_{ep} + d/\kappa_e} + \frac{1}{R_{p,Au}} \right)^{-1} + 2R_{pp} \tag{2}$$

where R_{Si} is the thermal resistance from the Si layer, R_{ep} is the thermal resistance from electron−phonon coupling within the Au layer, κ_e is the electron-contributed thermal conductivity of the Au layer, $R_{p,Au}$ is the phonon-contributed thermal resistance of Au, and R_{pp} is the interfacial thermal resistance (ITR) between Au and Si layers. Equation 2 is an approximation for the ITR, which assumes that the ITR originating from phonons from Au to Si and Si to Au is identical, hence the term $2R_{pp}$. It is worth mentioning that this assumption is not always accurate since phonon transport across a material interface is asymmetric in nature, which could result in different ITRs as explained by Li et al.[32]

Based on eqs 1 and 2, the ITR of the Au−Si interface (R_{pp}) at different temperatures can be indirectly extracted from the measured Au/Si ML κ values, which can be written as

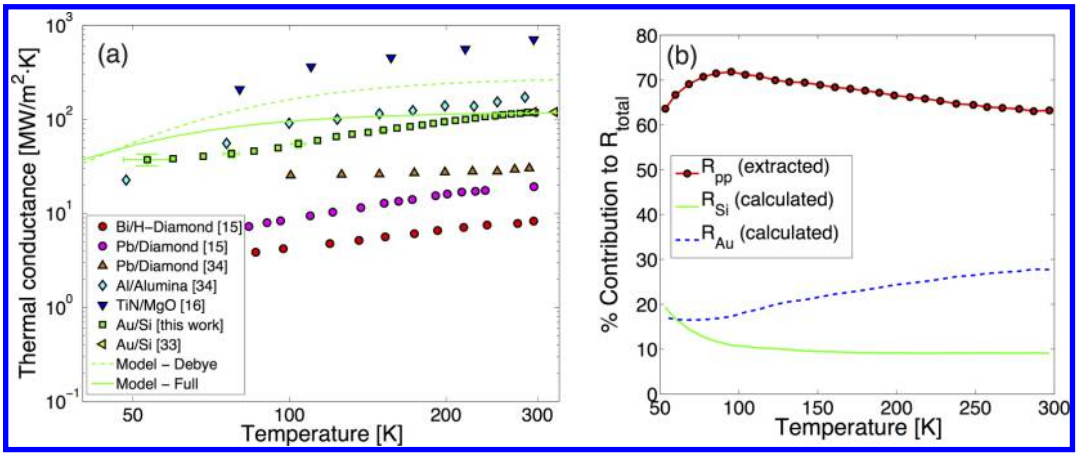

Figure 4. (a) Temperature-dependent data of previously measured interfacial thermal conductance in comparison to our extracted interface thermal conductance for Au/Si, which demonstrates a consistent temperature trend as in previous works (refs15, 16, 33, and 34). The DTR values for Bi/diamond, Al/Al_2O_3, and TiN/MgO are approximately 18.7, 2.1, and 1.6 respectively, while Au/Si has a DTR value of 3.9. As anticipated, the ITR of Au/Si lies between Al/Al_2O_3 and Bi/diamond. The dashed and solid green lines are the thermal conductance of the Au/Si interface calculated by DMM using the Debye approximation and full dispersion, respectively. The temperature-dependent trend for DMM is different from the measured conductance with a larger deviation at lower temperatures, which consequently manifests in the limitation of DMM in predicting ITR. (b) The relative contribution of ITR (R_{pp}), Si layer (R_{Si}), and Au layer (R_{Au}) to the total resistance for each Au/Si ML unit cell at various measured temperature points. The ITR of Au/Si is extracted from the measured κ of Au/Si ML and the calculated Si and Au film's thermal resistance as presented in this paper. Here, ITR is the primary contributor to the total thermal resistance and dominates the transport across the ML throughout the temperature ranges.

dx.doi.org/10.1021/nl500127c | Nano Lett. 2014, 14, 2448−2455

$$h_{pp,extracted} = 2\left(\frac{d_{total}/\kappa_{measured}}{N_{periods}} - R_{Si} - R_{Au}\right)^{-1} \quad (3)$$

where N is the total number of periods, d_{total} is the thickness of the ML film, R_{Si} is the calculated thermal resistance of a Si layer based on the minimum thermal conductivity model[14] (Supporting Information S5), and R_{Au} is the thermal resistance of a Au layer contributed by both electron and phonon pathways (Supporting Information S5–S6). Since R_{Si} and R_{Au} are based on theoretical calculations, the extracted h_{pp} summarized in Figure 4a should be taken as an estimation. Our Au/Si ML shows a similar thermal boundary conductance compared to previous Au/Si experiments[20,33] and has similar temperature dependency as in other reported works using different material systems.[15,16,34] Considering all thermal transport pathways, the ITR between Au and Si has the highest contribution, approximately ~60–75% to the total thermal resistance throughout the measured temperature range (Figure 4b). Within the Au layer, free electrons, which are the main heat carrier for bulk Au, are suppressed in the ML, and phonons in the Au film play a more dominant role in heat transport. The majority of thermal resistance in the electron pathway results from electron–phonon coupling ($R_e \ll R_{ep}$), and its thermal resistance is comparable to the phonon pathway in Au layer. Because Au is regarded as a "soft" material from a phonon standpoint, it inherently has low thermal conductivity if electrons play no role in heat transport, even lower than Si. Therefore, due to suppression of electron transport, there is no thermal pathway that can induce high thermal conduction as observed in bulk Au. To sum up, the combination of phonon-dominated transport in each layer and especially high ITR leads to an ultralow κ in the Au/Si ML. By degrading the interfaces in the annealed sample, the effect of ITR is substantially lessened and the κ of the "annealed" AuSi evidently enhanced.

We now focus on the understanding of the ITR and its comparison with the experimental data since it dominates the thermal transport in MLs.[2,4,35,36] The diffusive mismatch model (DMM), first proposed by Swartz and Pohl,[18] was used to model the thermal boundary conductance. A general form of thermal boundary conductance from materials A to B is defined as[18]

$$h_{A\to B} = \frac{\partial q_{A\to B}}{\partial T} = \frac{1}{4}\sum_{j=1}^{3}\int_{\omega} v_{A,j}(\omega)\,\alpha_{A\to B}(\omega)\,\hbar\omega\,\mathrm{DOS}_A(\omega)\frac{\partial f_o}{\partial T}\,d\omega \quad (4)$$

where h is the thermal boundary conductance, v_j is group velocity of mode j, $\hbar$ is Planck's constant, DOS is the phonon density of states, and f_0 is the Bose–Einstein distribution function. At the interface between material A and B following the detailed balance, phonon flux from A to B and from B to A must be equal. Phonons from A can either scatter back to A or transmit through B at the interface basing on the transmission probability. Different assumptions on the behavior of phonons as they interact with the interface lead to various formalisms for the transmission probability.[18,37−40] Within the framework of DMM, it is assumed that, once phonons hit the interface, they become completely diffusive.[18] In another word, phonons lose their memories in both directions and polarizations at the interface. Therefore, from the detailed balance $h_{A\to B} = h_{B\to A}$, the transmission probability can be defined as[18,22]

$$\alpha_{A\to B}(\omega') = \frac{\sum_j v_B(\omega')\,\mathrm{DOS}_B(\omega')\delta_{\omega,\omega'}}{\sum_j v_A(\omega')\,\mathrm{DOS}_A(\omega')\delta_{\omega,\omega'} + \sum_j v_B(\omega')\,\mathrm{DOS}_B(\omega')\delta_{\omega,\omega'}} \quad (5)$$

where $\delta_{\omega,\omega'}$ is the Kronecker delta, v is the group velocity for material A or B, and DOS is the density of states of material A or B. From eqs 4 and 5, the thermal boundary conductance can be calculated with known phonon dispersion relations.

For DMM calculations, phonon dispersion relations are needed for Au and Si. The Debye approximation, which is a linear approximation of phonon dispersion relation, has been used extensively due to its simplicity.[2,4,15,16] However, the Debye approximation is only accurate near the center of the Brillouin zone (BZ) and deviates significantly at the edge of BZ. Hence, such an estimation is only appropriate at temperatures much lower that the Debye temperature of the material considered. Reddy et al. pointed out the limitation of the Debye approximation and the importance of using full dispersion in DMM calculations.[22] Cahill et al.[4] and others also pointed out that the use of the Debye approximation may lead to an overestimation of the calculated interfacial conductance. In our Au/Si MLs, Au has a very low θ_D (θ_D = 165 K) when compared to most metals. Therefore, Debye approximation could be inaccurate for Au/Si MLs especially at room temperature.

To assess the validity of the Debye approximation, we calculate thermal conductance values using the DMM model with both Debye approximation and full dispersion and compare them with the experimental data. The full phonon dispersion relation is modeled using the Born–von Karman lattice dynamical model.[22,41] The vibrational properties (eigenfrequencies and eigenvectors at different wavevectors) can then be solved from the secular equation, $|D(\vec{q}) - m\omega^2 I| = 0$, with known dynamical matrices. The dynamical matrices for the diamond cubic structure derived by Herman[42] and fcc metal derived by Thakur and Singh[43] were applied to calculate bulk (3D) phonon vibrational spectra of Si[44] and Au, respectively. The assumption in using bulk phonon dispersion may not be completely valid at lower temperatures where the phonon wavelengths are longer, which may be a factor contributing to the discrepancy between the model and experimental data at low temperature as we shall see later. Full phonon dispersions calculated in this paper were also verified with previous experimental results (see more details in the Supporting Information S4).

It should be noted that by using lattice dynamics to calculate phonon dispersion relation, one must assume that the material structure in consideration has a perfect crystallinity, whereas the Au and Si layers of the MLs studied here are amorphous. Therefore, this is a big assumption made in the present model. Nevertheless, in most materials, the DOS of crystallized structures and their amorphous forms are fairly comparable. For instance, in amorphous Si,[45] the shape of the DOS widens, and the peaks at different frequencies are not as pronounced as in its crystal structure.[46,47] Therefore, the overlapping region when considering the transmission probability across the interface could be altered when using the crystalline structure. On the other hand, the average speed of sound of crystalline Si and amorphous Si are similar when the amorphous Si is fully dense.[48−51] The density of an amorphous film relies heavily on the material preparation methods, where the introduction of voids and porosity reduces the material's speed of sound and can range from 53% (by sputtering)[52] to ~100% (by glow discharge with density nearly identical to crystalline Si)[48] of the

dx.doi.org/10.1021/nl500127c | Nano Lett. 2014, 14, 2448–2455

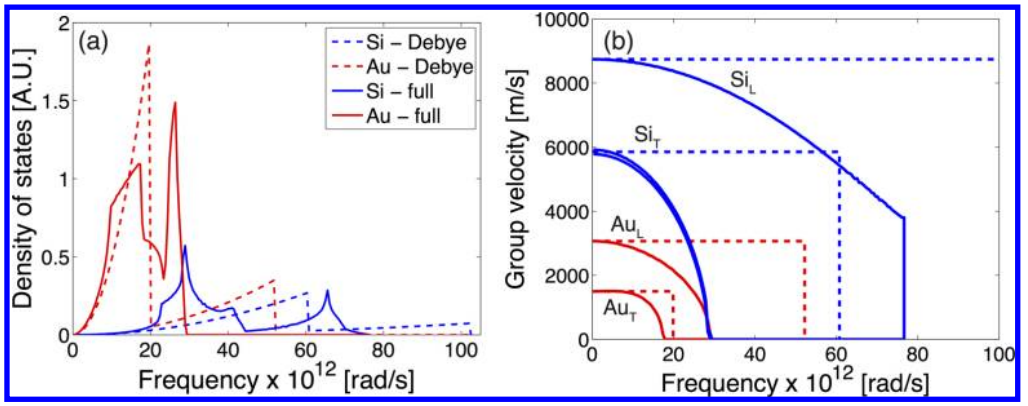

Figure 5. Phonon DOS (a) and group velocities (b) with respect to phonon frequency in Au (red) and Si (blue), respectively. Solid and dashed lines are based on full phonon dispersion and the Debye approximation, respectively, which agree well in both DOS and group velocity at low frequency but diverge at high frequency.

speed of sound of crystalline Si.[48−51] In addition, the speed of sound of 2−5 nm thin amorphous Si prepared by ion-beam sputtering to make Si/Mo MLs was measured indirectly and yielded 98% of its bulk's speed of sound.[53] The similar speed of sound between amorphous and crystalline Si suggests indifferences in group velocity in low-frequency phonons but could be different in the high-frequency regime. Nevertheless, one can also recognize that the phonon group velocity and DOS are closely related, as both are directly related to the derivative of the dispersion relations ($d\omega/dk$). The fact that DOS between a-Si and c-Si are similar to each other implies that the phonon group velocities between the two are probably similar. Since there is no work regarding the vibrational spectrum and group velocity of amorphous Au to our knowledge, we assume that the same phenomenon for Si also applies for phonons in Au. Even though the crystalline phonon dispersion cannot completely depict amorphous behavior of the thin film materials of interest, we believe that the full dispersion calculated from the lattice dynamics can still serve as a good approximation for the studied materials and is a more realistic representation compared to the Debye approximation.

From the dispersion relation, group velocity ($v_g = \partial\omega/\partial q$) and DOS are calculated numerically, as shown in Figure 5. At very low frequency, the Debye model gives a good approximation for group velocity and DOS in comparison to using full phonon dispersion. Hence, at low temperature where low frequency dominates phonon transport, both Debye approximation and full phonon dispersion are in good agreement with each other. However, at a higher frequency away from the acoustic region in BZ, full dispersion shows a lower group velocity compared to the Debye model, as evidenced in Figure 5b, which leads to overestimation in the thermal boundary conductance in the Debye model. In addition, discrepancies in DOS between the Debye and full phonon dispersion models are illustrated in Figure 5a. From the full phonon dispersion, van Hove singularities provoked by critical points in BZ are observed at different frequencies and does not follow parabolic trend as in the Debye approximation. From the differences in the calculated DOS and group velocity, we expect that the Debye approximation would overestimate the thermal boundary conductance between Au−Si interfaces. Therefore, using full dispersion to calculate thermal boundary conductance could explain the experimental data better.

By including the thermal conductivity of the Au and Si layers (see the Supporting Information S5), along with the calculated interfacial thermal conductance, we can model the total thermal resistance and the effective thermal conductivity of the MLs based on eq 1. Figure 3 shows the modeled effective thermal conductivities at different temperatures calculated for Au/Si MLs compared with the measured data. As expected, the Debye approximation is comparable to the full dispersion model at low temperature but overestimates the thermal conductivity at higher temperature by up to 1.6 times at room temperature. The modeling results with the full dispersion shows much better agreement with the experimental data for the entire temperature range of 30−300 K. It should be noted that no free parameter was employed in the calculation using DMM and the full dispersion. Therefore, this analysis indicates that the full dispersion, rather than the Debye model, could better capture the thermal transport across the Au/Si interface where Au has a low Debye temperature.

However, below 200 K, there are fairly large discrepancies between the DMM and experimental results. These discrepancies can be interpreted by considering the limitations and assumptions made in the present DMM model. First, as discussed earlier, dispersion relations of crystalline materials are used to model amorphous materials. Second, the model assumes perfect Au−Si scattering interfaces with no interdiffusion. However, roughness, imperfection, and bond strength between Au−Si in our fabricated MLs, which are not captured in the model, can contribute differently to the total thermal resistance.[9,20,54] Zhou et al.[54] carried out extensive modeling on the effect of interfacial morphology on ITR and found that interfacial roughness and diffused interface increase the interfacial conductance due to increased interface areas and the "phonon bridging" effect, respectively, whereas in our experiments, the thermal conductivity data below 200 K is lower than what is predicted by the DMM. This suggests that interface roughness or diffused interface is unlikely the cause of the discrepancy, as also evidenced by the clear interfaces observed in the TEM images and XRR peaks shown in Figure 1b and c. However, defects, such as impurities and voids, could still play a role as defect scattering is typically more pronounced in the intermediate temperature region. Third, DMM inherently assumes diffusive thermal transport across interfaces, which is not always true. High-frequency phonons, as opposed to low-frequency phonons, are more likely to be subject to diffusive processes; i.e., not all phonons participate in diffusive scattering. Since DMM stems from the diffusive behavior of phonons across an interface, it provides a better depiction of

phonon transport behavior at higher temperatures, where high-frequency phonons play a larger role. Therefore, a more substantial difference between experimental results and DMM in the low-temperature regime, where low-frequency phonons dominate, is observed. Furthermore, Landry and McGaughey,[55] based on both theoretical calculations and molecular dynamics (MD), showed that DMM could overestimate the interfacial thermal conductance if there is nondiffusive phonon scattering at interfaces between mismatched materials (Si and "heavy" Si in their case). In addition, the DMM model discussed here does not account for the inelastic scattering of phonons at interfaces, which is typically more pronounced at temperature higher than the material's Debye temperature. In our case of Au/Si ML, since the Debye temperature of Au is low, inelastic scatterings could play a role at an even temperature lower than room temperature. According to MD simulations from Landry and McGaughey's work and others,[39,55,56] thermal conductivity would increase monotonically with temperature in MLs at high temperature, whereas the elastic DMM model would lead to a plateau of κ vs T (see Figure 3). The temperature dependence of our experimental data seems to support the argument of inelastic phonon transmission. However, a further systemic study is warranted to further explore this point. Other than molecular dynamics simulations or analytical models, if the thickness of each layer in the ML structure is very thin, a quantum approach can also provide important insight regarding the underlying physics of metal/dielectric interfacial thermal resistances that the classical approach inadequately elucidates.[57,58]

Finally, to place our measured thermal conductivity of the MLs in perspective, we summarized the thermal conductivity values of various inorganic MLs reported to date, in corresponding to interface density, as shown in Figure 6. The color scale of each data point indicates the magnitude of DTR in accordance to the colorbar. For a particular interface density system, the interface of materials with larger DTR tends to have lower thermal conductivity. One exception is for GST/ZnO:SiO_2 where the respective layers already possess low intrinsic thermal conductivity.[8] For an interface density of ~0.2 nm^{-1}, our Au/Si MLs, having the highest DTR, exhibit the lowest thermal conductivity. Based on the trend shown in Figure 6, it is expected that even lower thermal conductivity can be expected in MLs with higher interfacial density and larger DTR as previously supported by both experimental and theoretical works.[1,4,8,9,32,57]

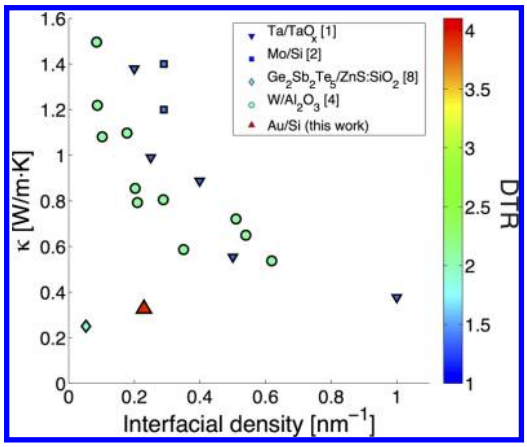

Figure 6. Summary of κ values for selected MLs with the corresponding interfacial densities. Data are taken from refs 1, 2, 4, and 8. The magnitude of Debye temperature ratio (DTR) of each data point is shown in the color bar, where red and blue indicate highest and lowest DTRs, respectively. As interfacial density increases, κ of MLs tends to decrease. With the same interfacial density, a material system with higher DTR tends to a have lower κ. One exception is GST/ZnS:SiO_2 ML where the individual layers possess an intrinsically low κ. The Au/Si ML in this work has the highest DTR among inorganic MLs measured to date and consequently shows a much lower κ compared to other MLs with the same interfacial density.

Conclusions. In conclusion, we demonstrated ultralow thermal conductivity in MLs made of Au and Si with a high interfacial density of approximately 0.2 nm^{-1} (the Au and Si layers are 5.7 and 3.0 nm, respectively). With a DTR of ~3.9, the Au/Si MLs represent the highest mismatched system in inorganic MLs measured to date. The measured thermal conductivity of 0.33 ± 0.04 W m^{-1} K^{-1} at room temperature is significantly lower than the amorphous limit of either Si or Au and is also much lower than previously measured MLs with similar interfacial density but lower Debye temperature ratios. The low Debye temperature of Au prompted us to examine the validity of the Debye approximation used in the theoretical analysis of interfacial thermal conductance. Our assessments suggests, in accordance with prior theoretical predictions, that full phonon dispersion could provide a better depiction of the measured interfacial thermal resistance in comparison to the Debye model. This work suggests that MLs with highly dissimilar Debye temperatures represent a promising approach to engineer thermal transport in inorganic MLs and achieve ultralow thermal conductivity.

■ ASSOCIATED CONTENT

Supporting Information

2D heat conducting model fitting for reference sample, influence of additional interfacial resistances in 3ω measurement, X-ray reflectivity data, validation of phonon dispersion relation of Si and Au, calculation of phonon-contributed thermal resistances of Si and Au layers, and calculation of thermal resistance due to electron−phonon coupling. This material is available free of charge via the Internet at http://pubs.acs.org.

■ AUTHOR INFORMATION

Corresponding Authors

*E-mail: efullerton@ucsd.edu (E.E.F.).
*E-mail: zhaowei@ucsd.edu (Z.L.).
*E-mail: rkchen@ucsd.edu (R.C.).

Notes

The authors declare no competing financial interest.

■ ACKNOWLEDGMENTS

This work was supported in part by the International Innovation Initiative and the CSRO program of Calit2 at UC San Diego, the Thermal Transport Program of the National Science Foundation (CBET-1336428), the Office of Naval Research (ONR) Young Investigator Award (N00014-13-1-0535), and the ONR MURI program (N00014-13-1-0678). We thank Prof. P. Reddy (Univ. Michigan) for sharing the codes of lattice dynamics to compute the phonon dispersions. We also thank S.W. Chen for help on XRR measurement.

REFERENCES

(1) Ju, Y. S.; Hung, M.-T.; Carey, M. J.; Cyrille, M.-C.; Childress, J. R. *Appl. Phys. Lett.* **2005**, *86* (20), 203113.
(2) Li, Z.; Tan, S.; Bozorg-Grayeli, E.; Kodama, T.; Asheghi, M.; Delgado, G.; Panzer, M.; Pokrovsky, A.; Wack, D.; Goodson, K. E. *Nano Lett.* **2012**, *12* (6), 3121−3126.
(3) Bozorg-Grayeli, E.; Li, Z.; Asheghi, M.; Delgado, G.; Pokrovsky, A.; Panzer, M.; Wack, D.; Goodson, K. E. *J. Appl. Phys.* **2012**, *112* (8), 083504.
(4) Costescu, R. M.; Cahill, D. G.; Fabreguette, F. H.; Sechrist, Z. A.; George, S. M. *Science* **2004**, *303* (5660), 989−990.
(5) Kyarad, A.; Lengfellner, H. *Appl. Phys. Lett.* **2004**, *85* (23), 5613−5615.
(6) Lee, S.-M.; Cahill, D. G.; Venkatasubramanian, R. *Appl. Phys. Lett.* **1997**, *70* (22), 2957−2959.
(7) Yang, B.; Liu, J. L.; Wang, K. L.; Chen, G. *Appl. Phys. Lett.* **2002**, *80* (10), 1758−1760.
(8) Kim, E.-K.; Kwun, S.-I.; Lee, S.-M.; Seo, H.; Yoon, J.-G. *Appl. Phys. Lett.* **2000**, *76* (26), 3864−3866.
(9) Jin, Y.; Yadav, A.; Sun, K.; Sun, H.; Pipe, K. P.; Shtein, M. *Appl. Phys. Lett.* **2011**, *98* (9), 093305.
(10) Liu, J.; Yoon, B.; Kuhlmann, E.; Tian, M.; Zhu, J.; George, S. M.; Lee, Y.-C.; Yang, R. *Nano Lett.* **2013**, *13* (11), 5594−5599.
(11) Ong, W.-L.; Rupich, S. M.; Talapin, D. V.; McGaughey, A. J. H.; Malen, J. A. *Nat. Mater.* **2013**, *12* (5), 410−415.
(12) Losego, M. D.; Blitz, I. P.; Vaia, R. A.; Cahill, D. G.; Braun, P. V. *Nano Lett.* **2013**, *13* (5), 2215−2219.
(13) Wang, X.; Liman, C. D.; Treat, N. D.; Chabinyc, M. L.; Cahill, D. G. *Phys. Rev. B* **2013**, *88* (7), 075310.
(14) Cahill, D. G.; Watson, S. K.; Pohl, R. O. *Phys. Rev. B* **1992**, *46* (10), 6131−6140.
(15) Lyeo, H.-K.; Cahill, D. G. *Phys. Rev. B* **2006**, *73* (14), 144301.
(16) Costescu, R. M.; Wall, M. A.; Cahill, D. G. *Phys. Rev. B* **2003**, *67* (5), 054302.
(17) Stoner, R. J.; Maris, H. J.; Anthony, T. R.; Banholzer, W. F. *Phys. Rev. Lett.* **1992**, *68* (10), 1563−1566.
(18) Swartz, E. T.; Pohl, R. O. *Rev. Mod. Phys.* **1989**, *61* (3), 605−668.
(19) Smith, A. N.; Hostetler, J. L.; Norris, P. M. *Microscale Thermophys. Eng.* **2000**, *4* (1), 51−60.
(20) Duda, J. C.; Yang, C.-Y. P.; Foley, B. M.; Cheaito, R.; Medlin, D. L.; Jones, R. E.; Hopkins, P. E. *Appl. Phys. Lett.* **2013**, *102* (8), 081902.
(21) Kittel, C. *Introduction to Solid State Physics*; Wiley: New York, 2004.
(22) Reddy, P.; Castelino, K.; Majumdar, A. *Appl. Phys. Lett.* **2005**, *87* (21), 211908.
(23) Cahill, D. G. *Rev. Sci. Instrum.* **1990**, *61* (2), 802−808.
(24) Lee, S.-M.; Cahill, D. G. *J. Appl. Phys.* **1997**, *81* (6), 2590−2595.
(25) Kim, J. H.; Feldman, A.; Novotny, D. *J. Appl. Phys.* **1999**, *86* (7), 3959−3963.
(26) Borca-Tasciuc, T.; Kumar, A. R.; Chen, G. *Rev. Sci. Instrum.* **2001**, *72* (4), 2139−2147.
(27) Poate, J. *Gold Bull.* **1981**, *14* (1), 2−11.
(28) Tadashi, I.; Yuuki, N.; Junji, E.; Dominique, C.; Hiroyuki, F. *Nanotechnology* **2009**, *20* (6), 065705.
(29) Cahill, D. G.; Katiyar, M.; Abelson, J. R. *Phys. Rev. B* **1994**, *50* (9), 6077−6081.
(30) Cahill, D. G.; Fischer, H. E.; Klitsner, T.; Swartz, E. T.; Pohl, R. O. *J. Vacuum Sci. Technol., A* **1989**, *7* (3), 1259−1266.
(31) Zink, B. L.; Pietri, R.; Hellman, F. *Phys. Rev. Lett.* **2006**, *96* (5), 055902.
(32) Li, B.; Lan, J.; Wang, L. *Phys. Rev. Lett.* **2005**, *95* (10), 104302.
(33) Oh, D.-W.; Kim, S.; Rogers, J. A.; Cahill, D. G.; Sinha, S. *Adv. Mater.* **2011**, *23* (43), 5028−5033.
(34) Stoner, R. J.; Maris, H. J. *Phys. Rev. B* **1993**, *48* (22), 16373−16387.
(35) Ordonez-Miranda, J.; Alvarado-Gil, J. J.; Yang, R. *J. Appl. Phys.* **2011**, *109* (9), 094310.
(36) Singh, P.; Seong, M.; Sinha, S. *Appl. Phys. Lett.* **2013**, *102* (18), 181906.
(37) Dames, C.; Chen, G. *J. Appl. Phys.* **2004**, *95* (2), 682−693.
(38) Hopkins, P. E. *J. Appl. Phys.* **2009**, *106* (1), 013508.
(39) Hopkins, P. E.; Norris, P. M.; Duda, J. C. *J. Heat Transfer* **2011**, *133* (6), 062401−062401.
(40) Duda, J. C.; Hopkins, P. E.; Smoyer, J. L.; Bauer, M. L.; English, T. S.; Saltonstall, C. B.; Norris, P. M. *Nanoscale Microscale Thermophys. Eng.* **2010**, *14* (1), 21−33.
(41) Born, M.; Huang, K.; Britain, G. *Dynamical theory of crystal lattices*; Clarendon Press: Oxford, 1954.
(42) Herman, F. *J. Phys. Chem. Solids* **1959**, *8*, 405−418.
(43) Thakur, V. K.; Singh, T. N. *Phys. Status Solidi B* **1986**, *135* (1), 67−73.
(44) Wei, S.; Chou, M. Y. *Phys. Rev. B* **1994**, *50* (4), 2221−2226.
(45) Kamitakahara, W. A.; Soukoulis, C. M.; Shanks, H. R.; Buchenau, U.; Grest, G. S. *Phys. Rev. B* **1987**, *36* (12), 6539−6542.
(46) Feldman, J. L.; Allen, P. B.; Bickham, S. R. *Phys. Rev. B* **1999**, *59* (5), 3551−3559.
(47) Feldman, J. L.; Kluge, M. D.; Allen, P. B.; Wooten, F. *Phys. Rev. B* **1993**, *48* (17), 12589−12602.
(48) Grimsditch, M.; Senn, W.; Winterling, G.; Brodsky, M. H. *Solid State Commun.* **1978**, *26* (4), 229−233.
(49) Vacher, R.; Sussner, H.; Schmidt, M. *Solid State Commun.* **1980**, *34* (5), 279−281.
(50) Tan, S. I.; Berry, B. S.; Crowder, B. L. *Appl. Phys. Lett.* **1972**, *20* (2), 88−90.
(51) Cox-Smith, I. R.; Liang, H. C.; Dillon, R. O. *J. Vacuum Sci. Technol., A* **1985**, *3* (3), 674−677.
(52) Testardi, L. R.; Hauser, J. J. *Solid State Commun.* **1977**, *21* (11), 1039−1041.
(53) Pu, N. W.; Li, T. C. *Appl. Phys. B: Laser Opt.* **2006**, *82* (3), 449−453.
(54) Zhou, X. W.; Jones, R. E.; Kimmer, C. J.; Duda, J. C.; Hopkins, P. E. *Phys. Rev. B* **2013**, *87* (9), 094303.
(55) Landry, E. S.; McGaughey, A. J. H. *Phys. Rev. B* **2009**, *80* (16), 165304.
(56) Duda, J. C.; Norris, P. M.; Hopkins, P. E. *J. Heat Transfer* **2011**, *133* (7), 074501−074501.
(57) Wang, L.; Li, B. *Phys. Rev. B* **2006**, *74* (13), 134204.
(58) Zhang, L.; Lu, J. T.; Wang, J. S.; Li, B. *J. Phys.: Condens. Matter* **2013**, *25* (44), 445801.